energies

MDPI

Article

A Novel DC-Bus Sensor-less MPPT Technique for Single-Stage PV Grid-Connected Inverters

Mohamed A. Elsaharty [1], Hamdy A. Ashour [1], Elyas Rakhshani [2], Edris Pouresmaeil [3,4,*] and João P. S. Catalão [3,4,5]

1 Department of Electrical and Control Engineering, College of Engineering and Technology, Arab Academy for Science, Technology & Maritime Transport, Alexandria 1029, Egypt; mohamed.atef.abbas.elsaharty@estudiant.upc.edu (M.A.E.); saharty@aast.edu (H.A.A.)
2 Electrical Engineering Department, Technical University of Catalonia (UPC), Barcelona 08034, Spain; elyas.rakhshani@gmail.com
3 University of Beira Interior, R. Fonte do Lameiro, 6201-001 Covilhã, Portugal; catalao@ubi.pt
4 INESC-ID, Inst. Super. Tecn., University of Lisbon, Av. Rovisco Pais, 1, 1049-001 Lisbon, Portugal
5 INESC TEC and Faculty of Engineering of the University of Porto, R. Dr. Roberto Frias, 4200-465 Porto, Portugal
* Correspondence: edris.pouresmaeil@gmail.com; Tel.: +34-671-319-249

Academic Editor: Gabriele Grandi
Received: 29 December 2015; Accepted: 21 March 2016; Published: 30 March 2016

Abstract: Single-stage grid connected inverters are considered as an economic, compact and simple topology compared with multi-stage inverters. In photovoltaic (PV) grid connected systems, the major requirement is to achieve maximum output power from the source. Maximum Power Point Tracking (MPPT) techniques require measurements on the DC side of the inverter connected to the PV in order to determine the current operating point on the power characteristics. Typically this is achieved by perturbing the reference output power and observe the change in the PV voltage, current or both. Based on the observation, it could be determined whether the current operating point is beyond or below maximum power. This paper presents an MPPT technique for a single-stage PV grid connected inverter where the MPPT algorithm determines the current operating point at different operating conditions based upon observing the inverter controller action. Such approach eliminates the requirement of sensing elements to be added to the converter which aids the advantages of the single-stage converter. Design of the utilized PV system is derived based on filter parameters, PV panel selection and controller parameters. Using simulation and practical implementation, the performance of the proposed MPPT technique is evaluated for the PV grid connected system.

Keywords: single-stage converter; MPPT technique; sensor-less; photovoltaic; grid connected

1. Introduction

Utilization of photovoltaic (PV) technology in grid-connected applications offers several advantages, including notable reductions in maintenance and pollution. Extraction of maximum power is considered the main priority in such systems, which is mainly dependent on sunlight intensity. Maximum Power Point Tracking (MPPT) techniques are required to detect and extract such operating points. In the literature, several topologies have been utilized for the integration of PV technology in grid connected applications, which include single stage (DC/AC) or two stage (DC/DC/AC) converters [1]. In practical implementation, reduction of power electronic switching devices, number of conversion stages and sensing elements are considered target design criteria in order to achieve a high efficiency, low cost and simplified system.

Among the possible selections of different topologies for grid connection of distributed energy sources, one of the simplest and cost effective topologies is the single-stage approach. Moreover,

such systems can be used in a micro-grid as a part of an energy management system [2–5]. In order for MPPT algorithms to determine and keep tracking at each instant the maximum operating point, measurements on the DC side of the inverter is required. Several approaches have been discussed in order to eliminate such measurements, thus reducing system complexity and cost. In [6–8] a sensor-less MPPT algorithm is proposed based on a two stage topology where the DC/DC converter tracks maximum power and DC/AC converter synchronizes and feeds the available power to the grid. However, such approaches require at least one measurement (voltage or current) on the DC side converter and involve excessive power switching devices as shown in Figure 1a. Meanwhile, other approaches discussed in [9–17] utilize a single-stage converter topology which benefits the reduction in number of conversion stages and power switching devices. However, as shown in Figure 1b, DC bus voltage and current are required by the MPPT algorithm in order to operate. Reduction of the number of sensing elements in single-stage topology has been discussed in [18] and the approach shown in Figure 1c was proposed based on only measurement of PV panel voltage for the MPPT algorithm to operate. It can be observed that these MPPT algorithms require at least one sensing element on the DC side of the converter which eventually requires filtering the measured values in order to obtain the average DC component thus requiring more processing power from the controller.

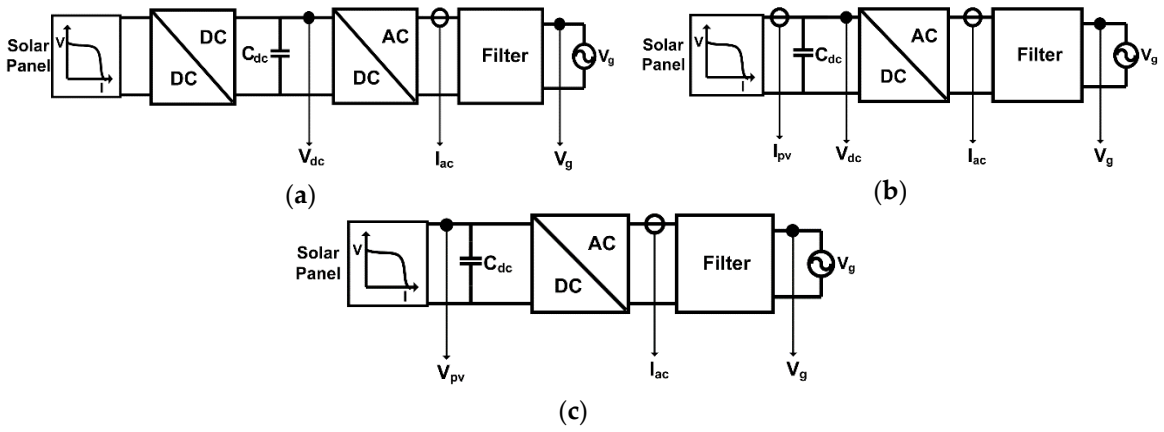

Figure 1. Typical configurations of PV grid connected system with (**a**) two stage converter, (**b**) single stage converter with two sensors on DC bus and (**c**) single stage converter with one sensor on DC bus.

Power filters are an essential stage in grid connected applications where current injected to the grid is required to comply with harmonic standards in electrical power systems. According to [19], LCL (T topology with two inductors and one capacitor) filters serve better decoupling and achieves high attenuation of high frequency harmonics caused by power electronics converter switching. However, filter components could limit the maximum output power of the system. Moreover LCL filters may cause both dynamic and steady state current distortions due to resonance. An L (inductor) filter may be a simple choice in terms of dynamic response and design, however bulky inductors and high switching frequencies are required to achieve harmonic standards.

With PV panels ranging in voltages from 23 to 45 V, it is hard to achieve voltage amplification in a single stage inverter without a line-frequency transformer. However, it is considered as an impractical component due to its increased size, weight and price. Modern inverter systems use high-frequency transformers requiring special design with integrated magnetic components and multi-stage conversion [20]. Another solution is the use of string technology where several PVs are connected in series so that the input voltage to the inverter circuit is high enough to avoid voltage amplification using certain topologies or transformer, hence increasing the overall efficiency. However, shading one of the PV modules would result in an overall reduction in the maximum power of the system.

In [21], a simple, fast, accurate, and easy-to-use modeling method was proposed for simulations of PV systems. The objective of the method was to identify the parameters of the non-linear I-V equation by adjusting the curve at the three points: open-circuit, maximum power and short circuit.

In this paper, in order to minimize the number of power electronics components used and simplify the topology, a current controlled, single-stage, single phase grid connected H bridge inverter topology is utilized [22,23]. Utilizing the concept described in [23], this paper presents design considerations for selection of PV panels, limitations in regards to operating range, tuning methodology of algorithm parameters and comparison to other operating scenario. A sensor-less MPPT algorithm is proposed and implemented based on perturbing the inverter reference output power and observing the inverter current controller action in order to maintain the required power without any sensors on the DC side. The phenomena of such an approach has been discussed in literature in [24] which reveals that by matching the dynamic resistance of a PV and static resistance MPP can be achieved. Utilization of such phenomena have been implemented in several references in several forms. In [25] an adaptive PV voltage control loop is proposed which makes use of estimation of the dynamic resistance. Model reference adaptive control has been proposed in [26] which takes into account the ripple correlation controller action in order to update the adaptive controller in order to minimize transient oscillations in system output voltage. An algorithm for reactive power compensation in PV systems based on observation of amplitude modulation index has been proposed in [27]. However, all these methods mainly depend on having a complex control structure and sensing PV voltage and/or current.

2. Derivation of the Proposed Technique

2.1. Typical Single-Stage Configuration Response

The setup shown in Figure 2 consists of a typical single-stage PV grid connected inverter. P_{ref} is the reference output power, m_a is the amplitude modulation ratio of the Sinusoidal Pulse Width Modulation (SPWM) technique, SW_1 and SW_2 are the inverter switches command signal, V_g and I_g are the grid voltage and current, respectively, V_{dc} and I_{dc} are the PV panel voltage and current respectively, V_i is the inverter output voltage, C_{dc}, R_1, L_1 are the dc link capacitor, filter inductor resistance and inductance, respectively.

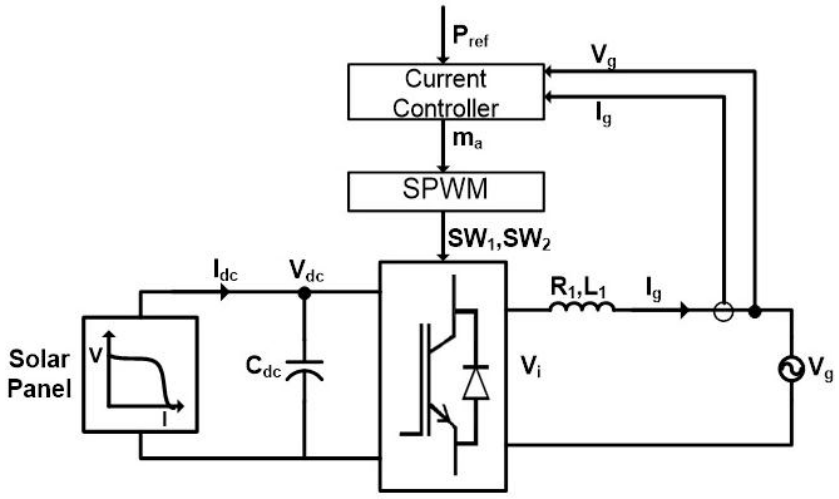

Figure 2. Configuration of single-stage, current controlled grid connected inverter.

Using Simulink under MATLAB the configuration in Figure 2 was simulated utilizing the PV modelling method discussed in [21]. Regulation of the DC bus voltage *i.e.*, PV panel voltage is achieved in conjunction with output power (P_{out}) regulation as shown in Figure 3. It can be observed that by increasing the reference output power (P_{ref}) in order to increase P_{out}, the inverter output voltage

(V_i) must be increased. This is achieved using the current controller by increasing the amplitude modulation ratio (m_a). This yields an increased output current (I_g) and increased dc current (I_{dc}) which consecutively causes a decrease in PV voltage (V_{dc}) according to the PV panel Power-Voltage characteristics shown in Figure 4. The PV panel would reach a particular operating point 1, 2 or 3 depending on P_{ref} while the inverter operating points are denoted by 1′, 2′ and 3′. During the first operating point 1 and 1′, P_{ref} is greater than zero which leads to a decrease in V_{dc} from the open circuit voltage of the PV and it can be observed that V_i is always less than V_{dc} due to the fact that the inverter operates in buck mode, thus m_a increases to m_{a1}. Assuming a sinusoidal grid current, voltage and unity power factor, the relationship between V_i, V_{dc} and m_a is given by:

$$V_i = m_a V_{dc} \tag{1}$$

$$|V_i| = \frac{\sqrt{\left(R_1 P_{ref} + |V_g|^2\right)^2 + \left(L_1 \omega P_{ref}\right)^2}}{|V_g|} \tag{2}$$

$$\delta = \sin^{-1} \frac{L_1 \omega P_{ref}}{|V_i|\,|V_g|} \tag{3}$$

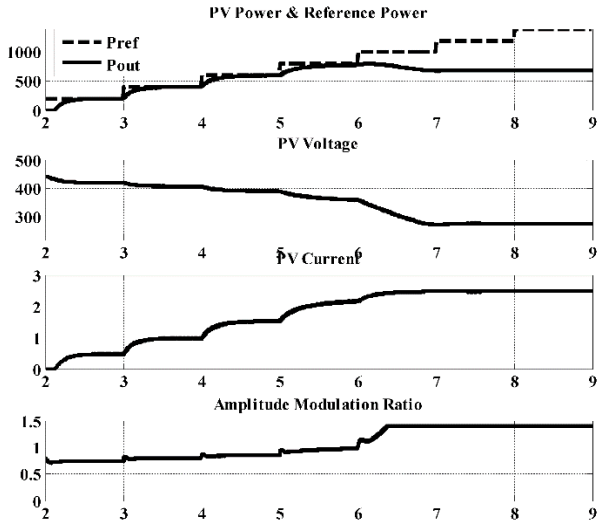

Figure 3. Typical response of a single-stage system with incremental reference power.

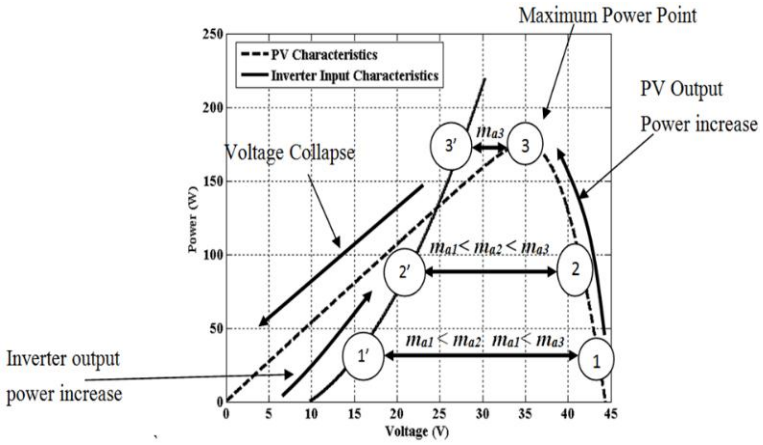

Figure 4. Inverter with filter characteristics at different operating points.

A similar reaction is observed when P_{ref} is increased to the operating point 2 and 2′. V_{dc} further decreases with excess output power due the PV characteristics while V_i increases to cope with line losses and inductor voltage drop, thus, according to Equation (1), m_{a1} would increase to m_{a2}. which is also illustrated in Figure 3 in Region 3–4. As P_{ref} is increased to the maximum power point at operating points 3 and 3′, the new amplitude modulation ratio m_{a3} indicates the minimum difference between V_{dc} and V_i. Meanwhile if P_{ref} is further incremented beyond this point, this indicates that the required P_{out} is beyond the maximum power point, the voltage would collapse as illustrated in Figure 3 in Region 6–9 and Figure 4.

In such a case, the current controller saturates, since to achieve the reference current magnitude, a greater output voltage is required by the inverter which the PV panel is incapable of supplying at that operating point which explains why m_a increases beyond the linear region of the inverter as shown in Figure 3. Thus, saturation of the current controller can be used as an indication to conclude that the P_{ref} is greater than the available PV maximum power. Typically the saturation value is set to 1, however in order to realize the current controller state at this particular operating point it is necessary to set the saturation value above 1 in order to make a definite conclusion that P_{ref} is beyond the maximum available power.

2.2. Effect of Change in Insolation

Among the factors that contribute effectively in affecting the available maximum power is the solar insolation. Insolation adjusts the PV characteristics yielding higher or lower maximum power point at different voltages as shown in Figure 5. To investigate the effect of changes in insolation on the current controller action, the following scenarios have been considered as the most feasible scenarios and illustrated in Figures 5 and 6:

1. Step increase in insolation while operating at or below the previous maximum power point;
2. Step decrease in insolation while operating below the new maximum power point;
3. Step decrease in insolation while operating above the new maximum power point.

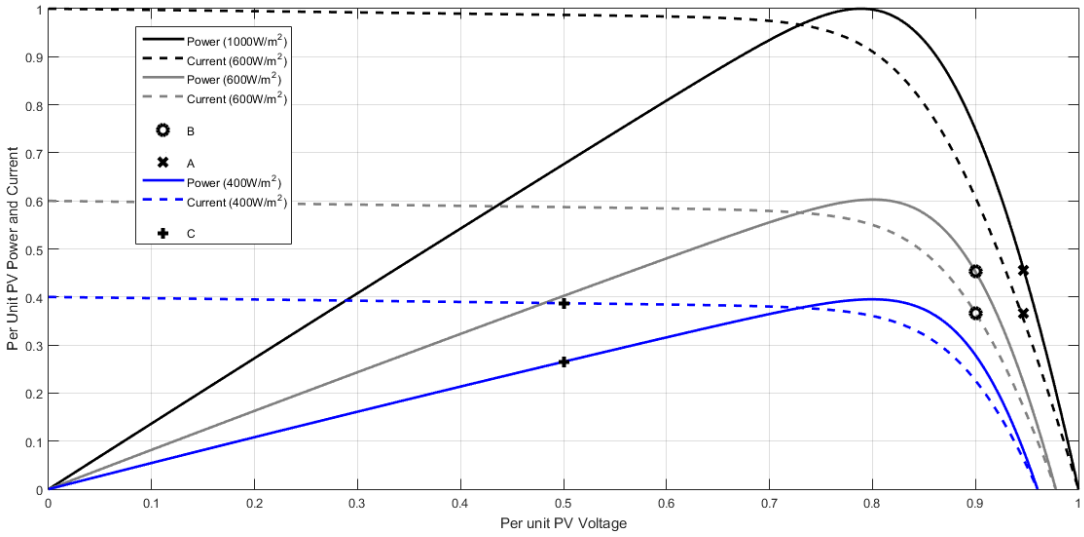

Figure 5. Effect of change in insolation on PV power and current characteristics at a particular operating point.

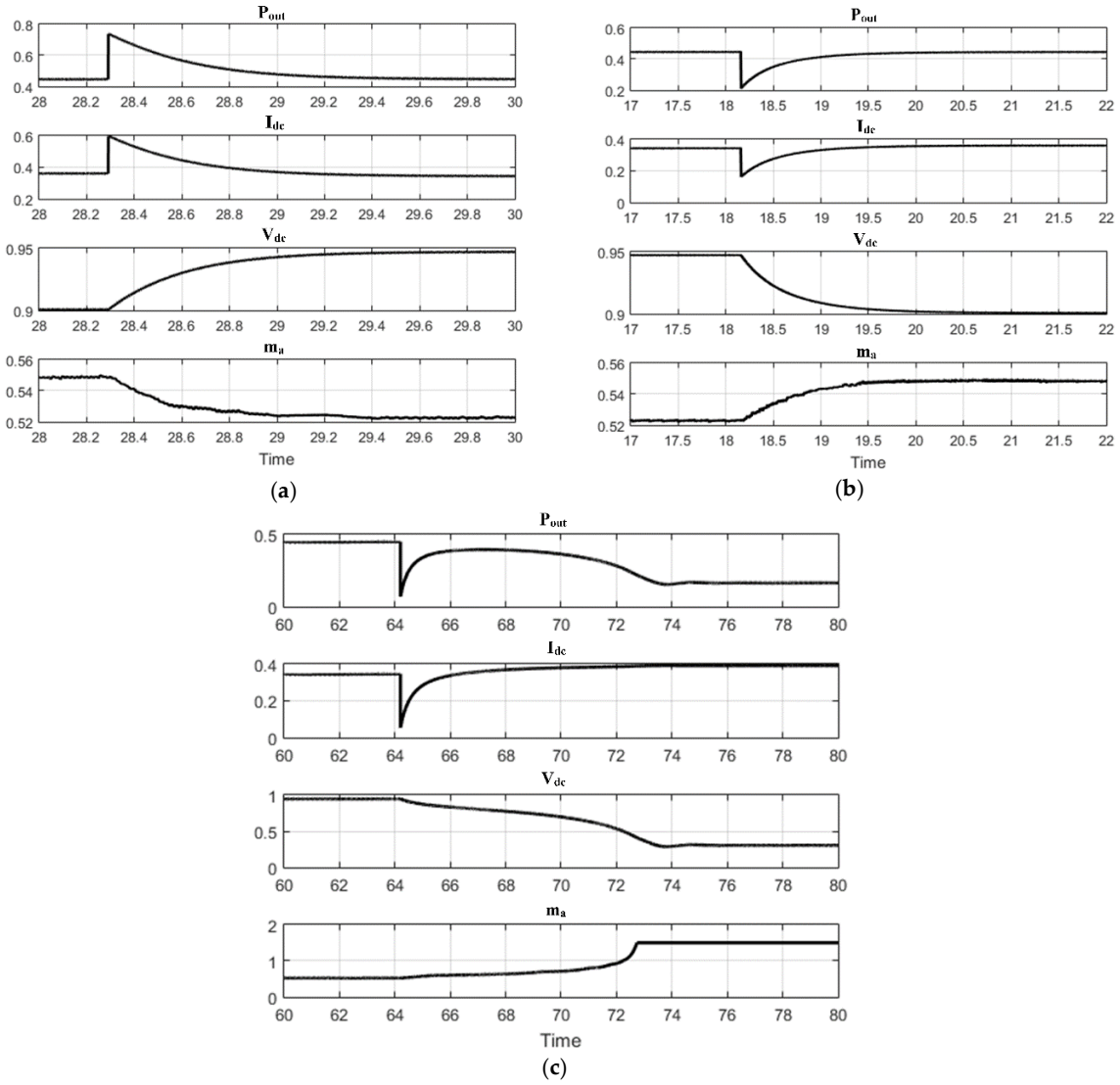

Figure 6. Per unit change in amplitude modulation ratio, PV voltage, current and power for (**a**) increase in insolation below the maximum power point (Point B to A), (**b**) decrease in insolation at a fixed reference power below the maximum power point (Point A to B) and (**c**) decrease in insolation at a fixed reference power above the maximum power point (Point A to C).

Considering the first scenario, the insolation is increased from 600 to 1000 W/m^2 while operating at 0.45 per unit of the maximum power. The effect can be noticed in Figure 5 where the new operating point A voltage is greater than the previous characteristic curve operating point B. Since the available voltage on the DC bus has increased, the current controller reduces m_a in order to maintain the same output power as shown in Figure 6a.

The second scenario has an exact opposite effect of the first scenario since the new operating point B voltage is less than the previous characteristics curve operating point A. Since the available voltage on the DC bus has decreased, the current controller increases m_a in order to increase the output voltage and maintain the same output power as shown in Figure 6b.

The last scenario illustrated in Figure 5 as the movement from point A to C where previous output power was greater than the new maximum power. This yields to a voltage collapse due to the current controller increasing m_a to try to maintain the reference output power which eventually saturates the current controller as in Figure 6c. As mentioned earlier, the saturation value has to be set greater than 1 in order to make such a definite conclusion. In Figure 6c the saturation value was set at 1.5.

From this analysis it can be concluded that the current controller action can indicate the PV operating point. Thus it can be concluded that m_a can be taken as an indicator for the PV operating region without any measurements on the DC side of the inverter. Depending on the current control algorithm, the saturation limit can be estimated and m_a can be used as a feedback variable for the MPPT algorithm to determine the next consecutive action.

2.3. PV Selection Limits

In order for the grid connected inverter to achieve the PV panel maximum power point, a design criterion has to be satisfied. Assuming a loss-less inverter, P_{out} and the inverter power (P_{in}) can be considered equal. During normal operation, P_{ref} is equal to P_{in} which can be calculated using Equations (2) and (3). To select a suitable PV panel and in order to achieve maximum PV output power, V_i should be less than or equal to the PV voltage (V_{MPP}) at maximum output power (P_{MPP}). Figure 7 represents several PV panel's P_{MPP} at 1000 W/m^2 insolation. It can be observed that the "Possible Selections" region satisfies the design criteria mentioned earlier. This is an essential design criterion, since if the designed inverter and filter require a voltage greater than V_{MPP} in order to achieve an inverter output power of P_{MPP}, the system will never achieve true MPPT and the controller would saturate at an operating point below the P_{MPP} as illustrated in Figure 7 with the "Invalid Selection" region. The maximum amplitude modulation ratio (m_{amax}) can be calculated using the following equation:

$$m_{a\ max} = \frac{V_i|_{P_{MPP}}}{V_{MPP}} \tag{4}$$

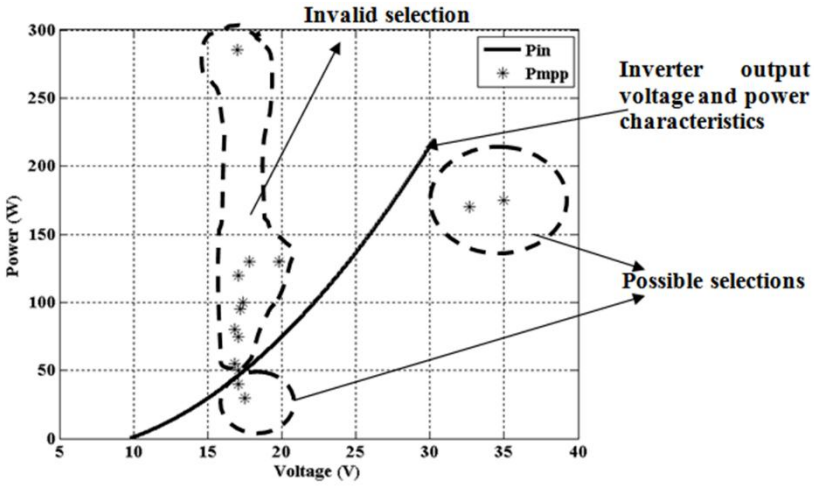

Figure 7. Example of inverter and several PV panels' power-voltage characteristics.

Changes in insolation would affect P_{MPP} and V_{MPP}. In order for the inverter to be capable of achieving maximum power at different operating conditions, P_{MPP} at these operating conditions should be achievable at a voltage greater than the required V_i. Considering one of the possible selections in Figure 7, the maximum power characteristics under different insolation is represented in Figure 8. It can be observed that at very low insolation, the inverter is unable to output P_{MPP} since V_{MPP} is below the operating voltage for that power. In such case the *MPPT* algorithm design is set to either:

- Continue operation at a power point below the maximum power as long as the inverter and PV voltage criteria are satisfied.
- Set a cut-off power for the inverter such that the inverter will cease operation at very low power values.

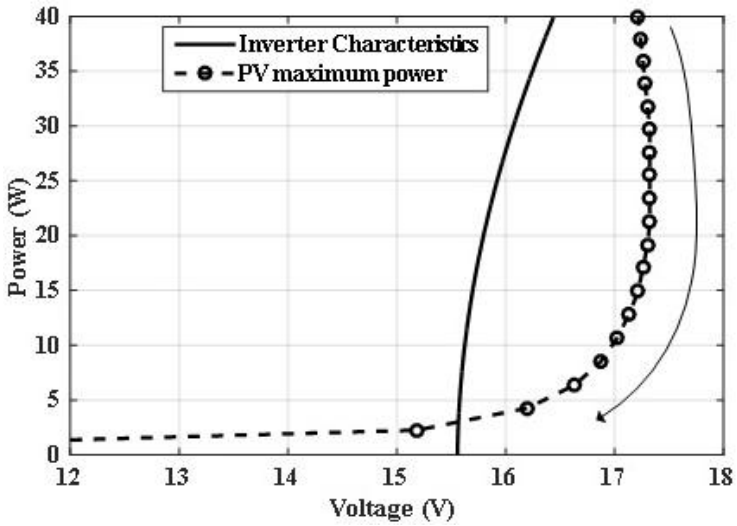

Figure 8. Example of inverter and PV characteristics of a PV panel at different insolations (arrow direction indicates decrease in insolation).

3. Proposed System

3.1. Configuration

The proposed setup is illustrated in Figure 9, perturbation to the inverter reference output power is achieved by analyzing the feedback information from m_a. The MPPT algorithm will be executed periodically to compare the previous and current state of the controller in order to determine the next consecutive action.

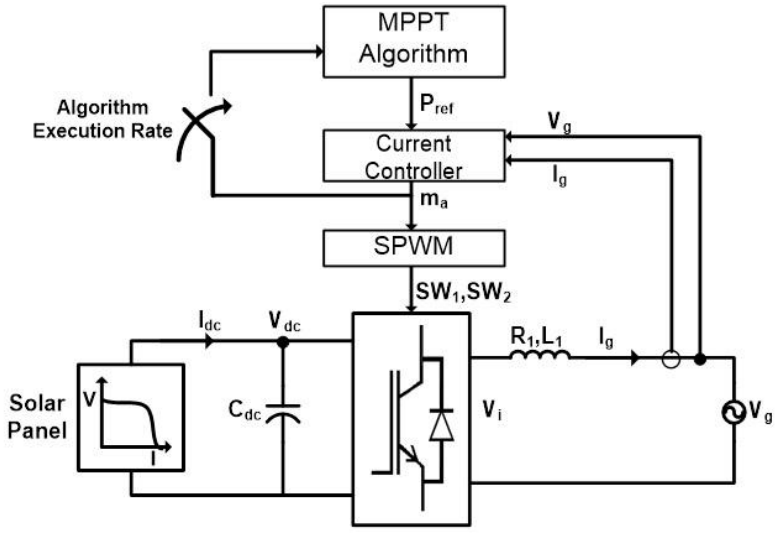

Figure 9. Proposed setup for sensor-less grid connected inverter.

3.2. Algorithm

The MPPT algorithm shown in Figure 10 explains the method of decision making of increment/decrement reference power of the inverter, based on the feedback m_a. The algorithm logic is based upon the following three processes:

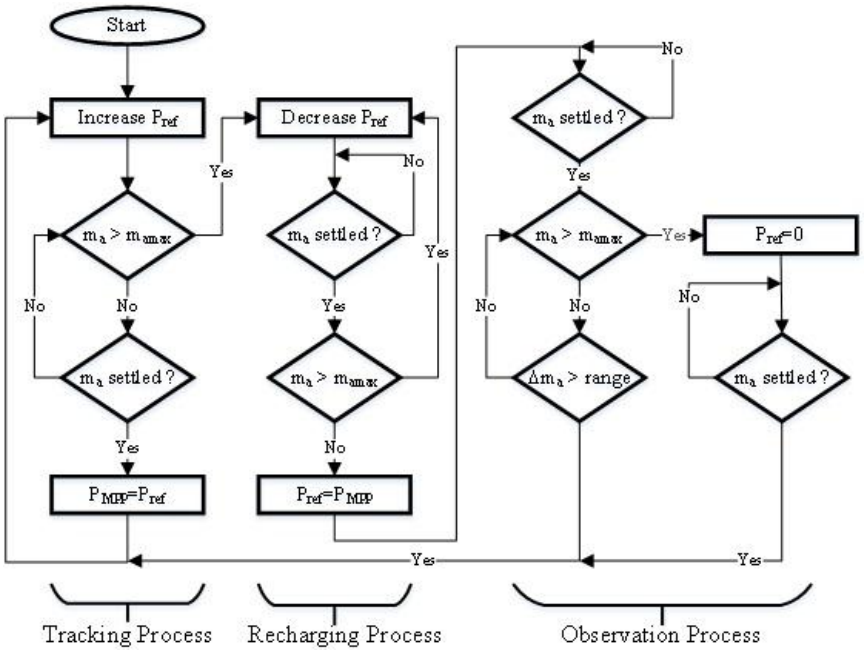

Figure 10. Flowchart of the proposed MPPT algorithm.

3.2.1. Tracking Process

The Tracking Process is executed by incrementing P_{ref} on regular basis while m_a is observed. When m_a increases beyond the permissible maximum (m_{amax}), the next process is executed. In order for an increment to be executed, it is necessary that m_a is in steady state by checking if it is oscillating with a tolerance band. This is necessary in order to avoid the algorithm incrementing several consecutive times while the current controller is slowly catching up due to slow dynamics of the system or controller, thus yielding a reference power point far beyond the actual. Once m_a is considered settled in the steady state tolerance band, the current reference output power is considered the maximum power and the algorithm increments the reference output power to repeat the observation. An increase of m_a to m_{amax} would indicate that this reference output power is beyond the maximum power and the inverter is tending towards instability as discussed in Section 2.1. Thus the algorithm leaves the Tracking Process since it is known now that the previous reference output power is the maximum output power.

3.2.2. Recharging Process

In this process the current controller is reset to a stable point by consecutively reducing the reference output power. By observing m_a the converter stability is detected at which point it executes the next process. Due to the Tracking Process final state the DC Bus has started collapsing as explained earlier in Section 2.1 and it is necessary to recharge the DC link capacitor. By reducing P_{ref}, the absorbed power from the PV is reduced thus allowing the voltage to increase back to be within the inverter operation limits as shown in Section 2.3. Since the last stored reference power is the maximum power, the inverter is set to operate at this power and the algorithm shifts to the next process to observe any changes.

3.2.3. Observation Process

This final process constantly tries to detect any changes to environmental conditions that can affect the maximum output power. If maximum power is increased the algorithm goes back to the Tracking Process, while if the maximum power is decreased then the inverter is reset and the program is re-executed.

As discussed in Section 2.2, an increase of m_a indicates a decrease in insolation and *vice versa*. Thus if m_a decreases, the algorithm would re-execute the Tracking Process in order to continue tracking to the new maximum power, whereas if m_a increases in this process, it is obvious that the inverter will tend to instability since the P_{ref} is higher than the new maximum power. Thus m_a will increase to m_{amax} and in this case the sequence is reset by setting P_{ref} to zero, waiting for the inverter to stabilize and starting up the Tracking Process again.

Considering the analysis in Section 2.3 at low insolations, the algorithm will operate at a power point below the maximum. This is due to the fact that in this scenario the maximum power point is achieved at a lower voltage than the inverter operating voltage for such power. Meanwhile, if the maximum power is below P_{ref} increment value, the inverter operating point will be zero which means the inverter has seized operation until any changes occur to m_a which indicates an increase in insolation i.e. an increase in available power.

3.3. Controller

The controller action is required to have a minimum overshoot. This is essential in order to avoid m_a increasing beyond m_{amax} during the Tracking Process. The controller shown in Figure 11 illustrates the implemented controller structure. The controller consists of an error integrator, which compares the required grid current and actual grid current. The integrator eliminates the error caused by the variable DC bus voltage due to the non-linear V-I characteristics and changes to operating conditions of the PV panel. The integral gain (K_i) is required in order to achieve zero steady-state error between reference (I_g^*) and actual grid current (I_g). The controller action in this form ensures minimum overshoot and zero-steady state error [28–31].

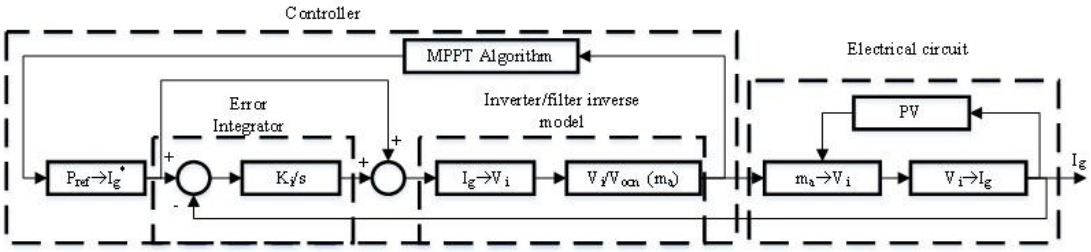

Figure 11. Current controller for sensor-less technique.

3.4. Parameters

Three parameters in the algorithm are required to be adjusted in order for it to operate in the required manner: *settlement range*, *algorithm sampling rate* and *reduction range* as shown in Figure 12. The *settlement range* is the tolerance band over which m_a oscillates during operation and as long as m_a is oscillating within this band then it is considered to be settled. In Figure 12 the algorithm is shown in the Observation Process from Regions 1 to 4. In the Observation Process, the algorithm checks that m_a did not change. In case m_a is outside this *settlement range*, m_a would be considered as unsettled and the algorithm waits for m_a to settle to determine the next consecutive action. In Regions 5 to 8, the insolation is increased which yields a decrease in m_a and the algorithm would detect a reduction in m_a beyond the preset *reduction range* which is greater than the *settlement range*. At this state the algorithm waits for m_a to settle again within the *settlement range* to restart the Tracking Process. In Regions 9 to 12, the algorithm starts the Tracking Process by perturbing and observing m_a to settle again. The *algorithm sampling rate* is set so that it should be slower than the controller time constant (K_i), so that sufficient time is given to the controller to settle before the algorithm shifts to another state.

In order to estimate the required *reduction range* due to insolation and/or temperature changes, a model based approach is used to determine this parameter. The PV model in [21] is represented by Equation (5), where I_{dc} and I_o are the PV and saturation currents respectively, V_t is the thermal voltage, R_s and R_p are the equivalent circuit series and parallel resistance of the PV model.

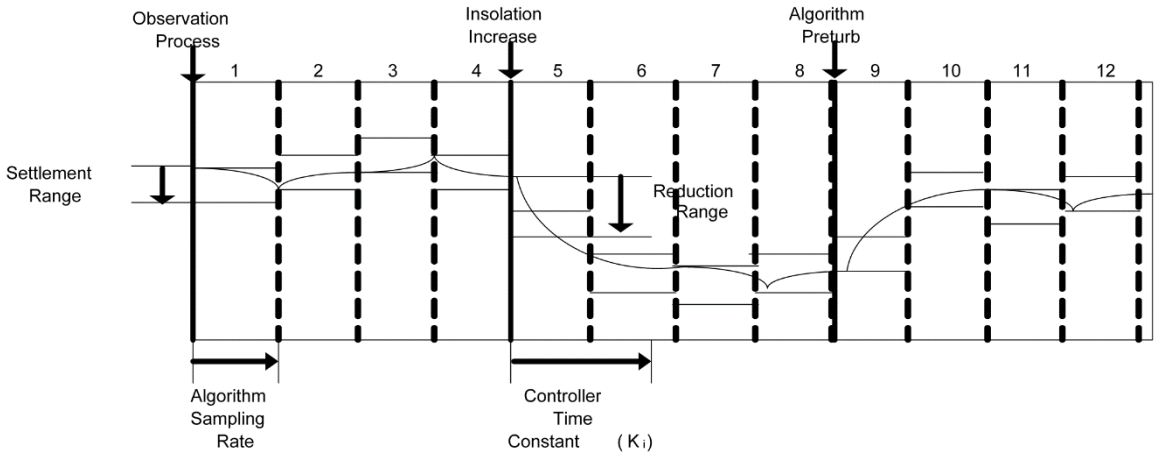

Figure 12. Graphical representation of algorithm tuning parameters.

$$V_{dc} = I_{dc} - I_o \left(e^{\frac{(V_{dc} + \frac{R_s P_{out}}{V_{dc}})}{V_t}} - 1 \right) - \frac{P_{out}}{V_{dc}} \left(R_s + R_p \right) \quad (5)$$

In Figure 13, as the insolation increases, the controller copes with the change by adjusting the amplitude modulation ratio to m_{a2} where $m_{a2} < m_{a1}$. The MPPT algorithm is required to detect the change in amplitude modulation ratio (Δm_a) in order to recognize that a new maximum power is available. A small change in insolation would lead to a decreased Δm_a and *vice versa*.

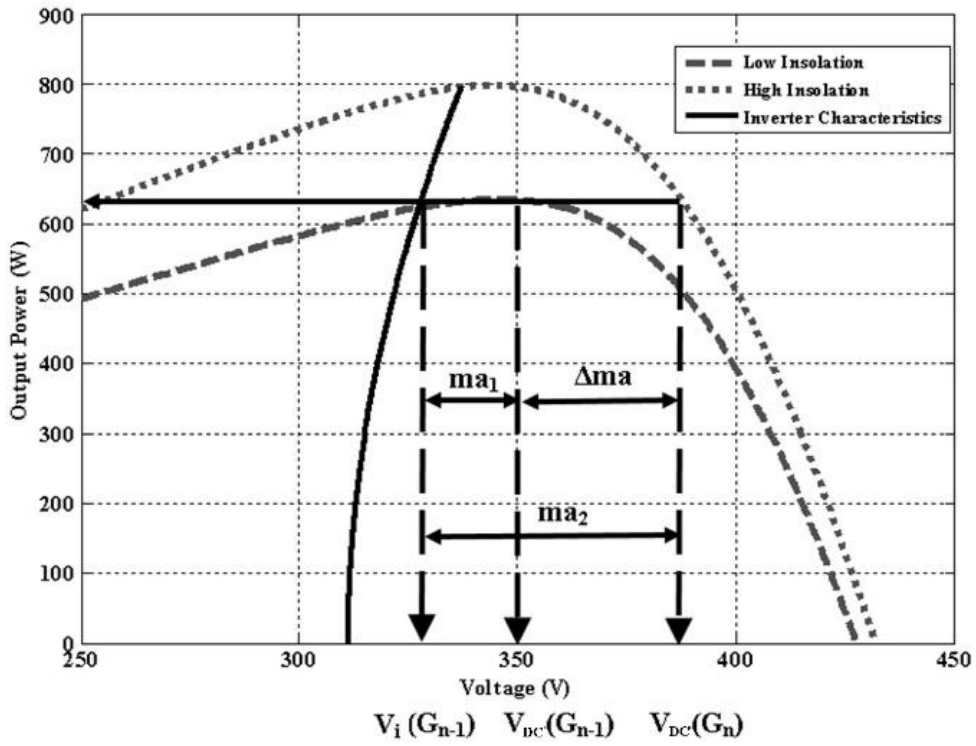

Figure 13. Change in amplitude modulation ratio due to change in insolation.

Change in m_a is described in Equation (6) where $V_i(G_{n-1})$ represents the inverter voltage to obtain the maximum output power at low insolation (G_{n-1}) while $V_{dc}(G_{n-1})$ is the PV voltage at that insolation. As insolation increases from G_{n-1} to G_n, the PV voltage at which the same output power is required increases to $V_{dc}(G_n)$. Using PV characteristics at different insolations and temperatures combined with the inverter characteristics a relationship can be established between changes in insolation ΔG, Δm_a at several temperatures T.

$$\Delta m_{ak} = \frac{V_i\left(G_{n-1}\right)}{V_{dc}\left(G_n\right)} - \frac{V_i\left(G_{n-1}\right)}{V_{dc}\left(G_{n-1}\right)} \tag{6}$$

The relationship shown in Figures 14 and 15 shows the effect of ΔG, Δm_a at different insolation changes ΔG_n as shown in Equation (7). It can be noticed that the minimum Δm_a is satisfied at changes in high insolation values ΔG_n. Moreover, at very low changes to insolation ΔG the difference further decreases. Thus the algorithm minimum change in m_a can be calculated using Equation (6) by:

1. Choosing a suitable ΔG: this is a design selection based on the required sensing of changes in insolation. Decreasing the value of ΔG leads to an increased accuracy of obtaining true maximum power.
2. Find $V_{dc}(G_{n-1})$ and $P_{out}(G_{n-1})$: using PV model in Equation (5), calculate the PV maximum output power at nominal temperature and insolation below maximum by ΔG.
3. Find $V_{dc}(G_n)$: calculate the PV voltage at maximum insolation that would give the same output power at the lower insolation calculated earlier:

$$\Delta G_n = G_n - G_{n-1} \tag{7}$$

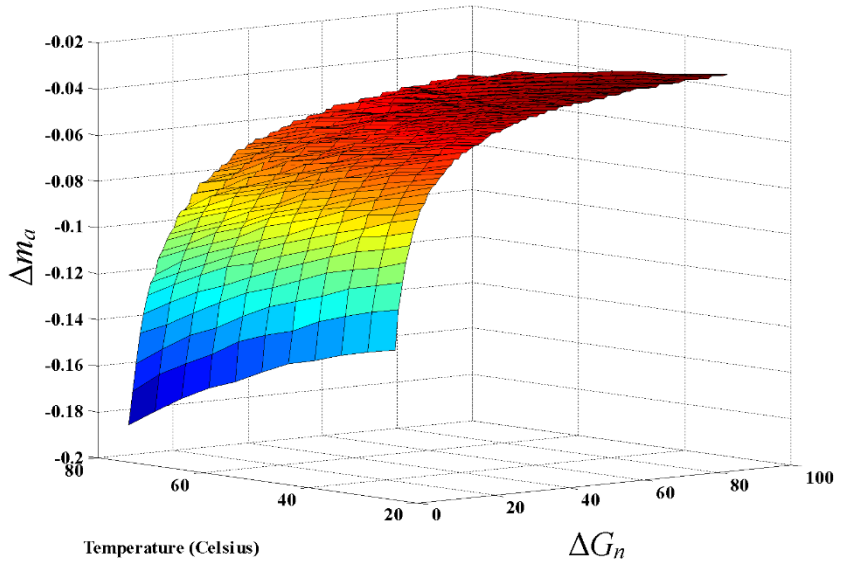

Figure 14. Change in amplitude modulation ratio due to change in insolation and temperature for ΔG = 10.

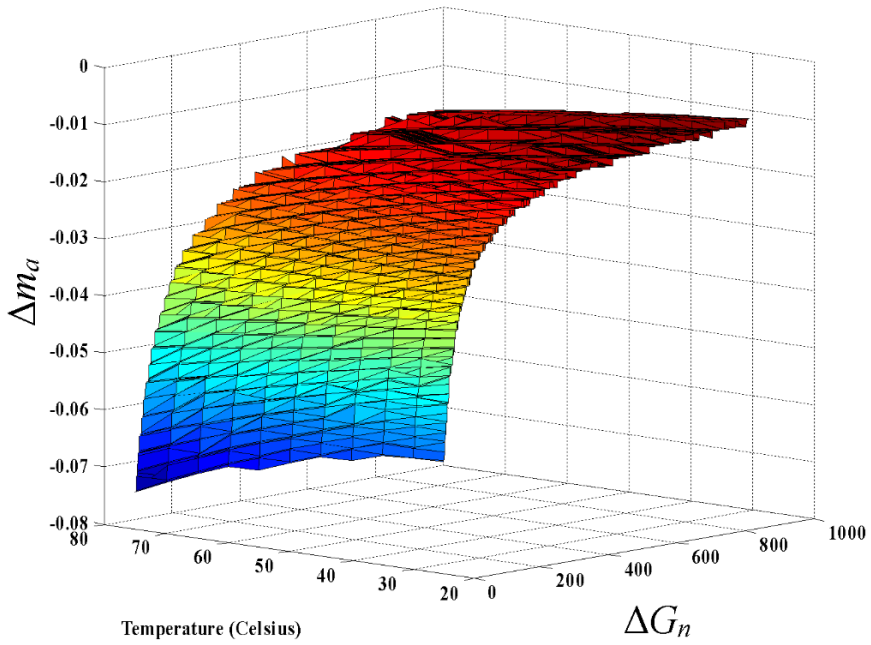

Figure 15. Change in amplitude modulation ratio due to change in insolation and temperature for $\Delta G = 1$.

4. Simulation Results

The algorithm was implemented on a system with the specifications shown in Table 1. The system was checked prior to simulation that it satisfies the design criteria. The inverter voltage was calculated using Equation (2) for the entire operating range and checked to match the PV output voltage throughout the range as shown in Figure 16. The L-filter design has been adopted based on the method introduced by the authors in [32].

Table 1. Simulated system parameters.

Parameter	Value
V_g	220 V_{rms}
Number of series PV modules	20
PV array total maximum power	800 W
L_1	80 mH
C_{dc}	10 mF
m_{amax}	0.98
Settlement range	$\pm$0.002
Δm_a	0.005
algorithm sampling rate	0.1 s
K_i Sensorless configuration	8.0
K_p Sensored configuration (Voltage control loop)	0.5
K_i Sensored configuration (Voltage control loop)	2.2
K_p Sensored configuration (Current control loop)	0.4
K_i Sensored configuration (Current control loop)	8.0
Sensorless configuration reference power increment	70 W
Sensored configuration reference voltage increment	1 V

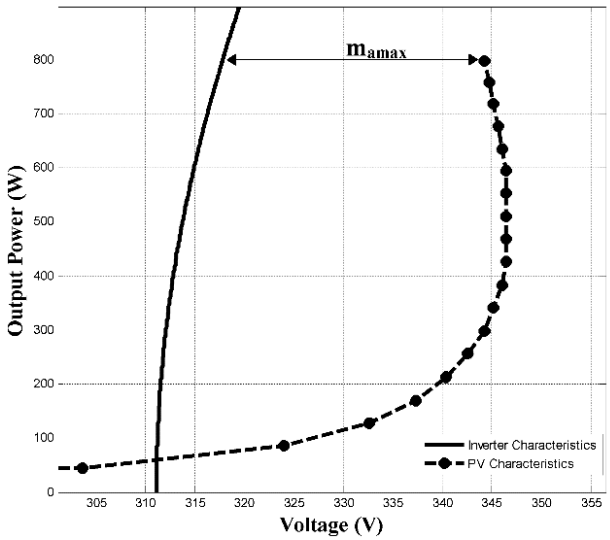

Figure 16. Selected inverter and PV maximum power at different insolations (0 to 1000 W/m^2 in increments of 50 W/m^2).

4.1. Proposed Sensor-less Configuration

Simulation block diagram shown in Figure 17 consists of three main blocks. The MPPT Algorithm block implements the algorithm using a code-based approach. The input to the algorithm is filtered such that minor oscillations in m_a are not detected and sampled. The feedback grid current block consists of a Phase Locked Loop (PLL) to determine the grid voltage phase to transform the current to equivalent *dq* quantities. Conversion of reference *dq* inverter voltage to m_a in αβ reference frame as shown in Figure 17. In Figure 18, the power circuit is shown consisting of an H-bridge inverter and PV model with changing insolation with time.

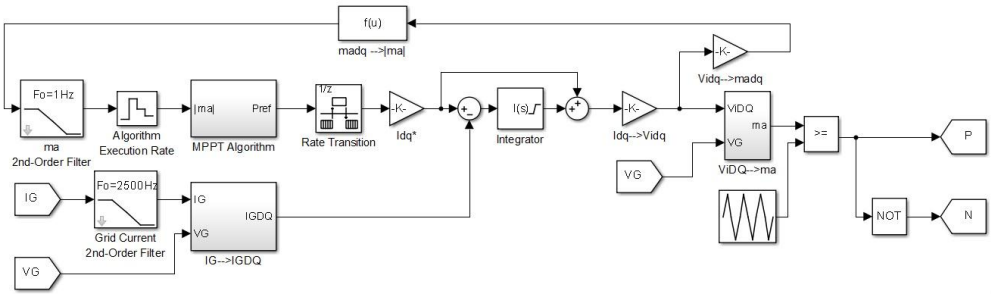

Figure 17. Simulation block diagram of the proposed sensor-less control structure.

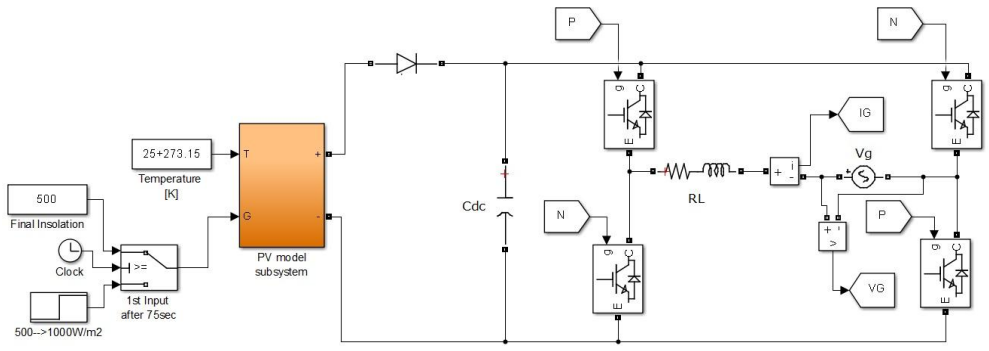

Figure 18. Simulation power circuit of proposed sensorless configuration.

The simulation results shown in Figure 19, shows that the algorithm is able to track the maximum power point under different operating conditions. In Figure 19, during the beginning of the simulation, the DC link capacitor charges up from 0 to 3 s. The algorithm starts Tracking Process until 22 s where m_a shown in Figure 20a increases beyond the maximum pre-set limit due to the voltage collapse shown in Figure 20b.

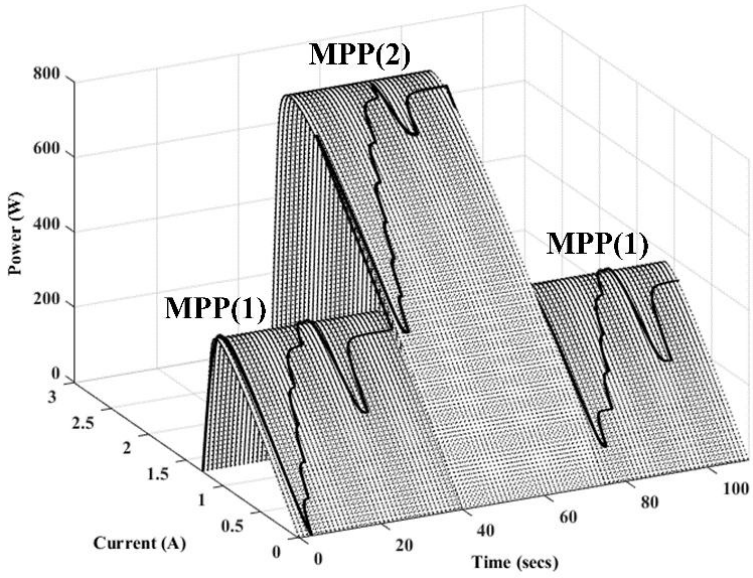

Figure 19. Proposed sensorless MPPT algorithm simulation as insolation increases after 15 s and decreases after 27 s.

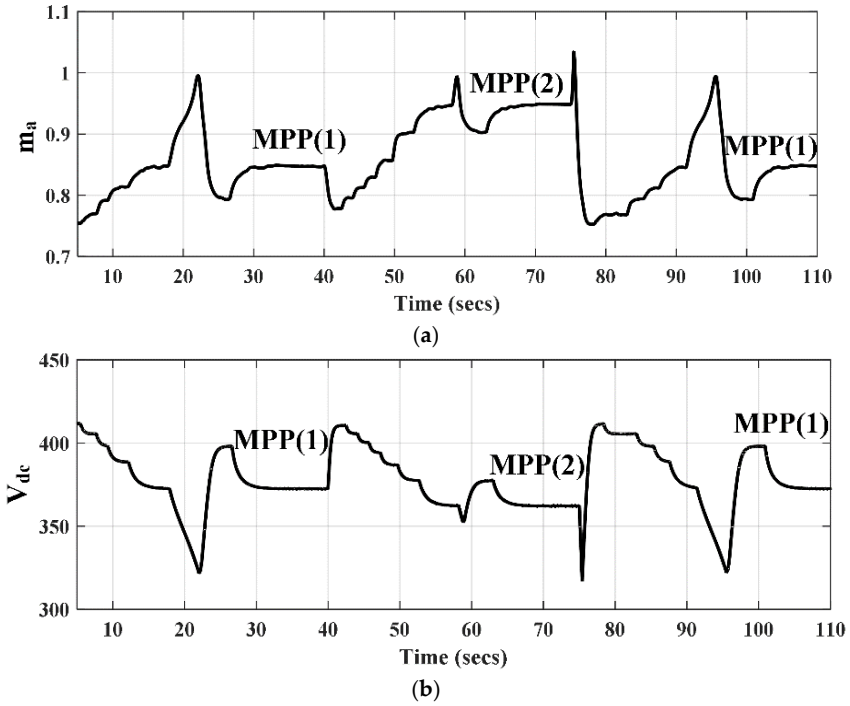

Figure 20. Simulation results of (**a**) Amplitude modulation ratio and (**b**) DC link voltage during algorithm operation.

The algorithm switches to recharging process during 22 to 26 s of simulation time where the capacitor recharges in this region as illustrated in Figure 20b. After 26 s, m_a has decreased and settled, therefore the algorithm shifts to the Observation Process where the algorithm sets the controller to operate at the previous maximum operating point MPP(1) before the voltage collapsed and maintains the current operating point as illustrated in Figure 19 during 26 to 40 s.

After 40 s, the insolation is increased to 1000 W/m^2. The algorithm detects this change by observing the decrease in m_a as shown in Figure 20a and the algorithm returns to the Tracking Process repeating the entire sequence up to the Observation Process again from 40 to 75 s MPP(2).

After 75 s, the insolation is decreased to 500 W/m^2. Since the current operating point is beyond the PV panel output power at the current operating conditions, the voltage collapses again in this scenario and m_a increases beyond m_{amax}. The algorithm shifts to zero output power and waits for m_a to settle while the DC link capacitor recharges. The Tracking Process is then restarted again in order to achieve maximum power at the new insolation MPP(1).

The output grid current is illustrated in Figure 21 where a larger output grid current is achieved at increased insolation MPP(2) and a reduced output grid current at low insolation MPP(1) and MPP(2). The instance where the output grid current is minimum represents the Recharging process of the algorithm. The Tracking process can be observed by the ramp increase in the output grid current.

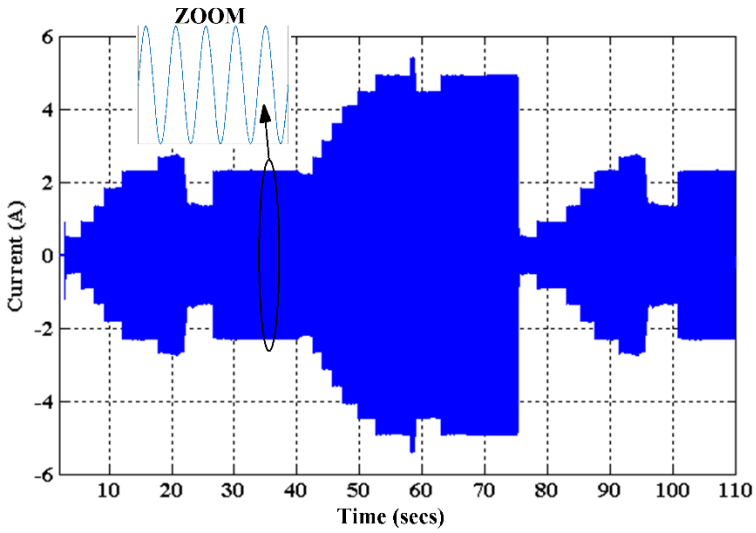

Figure 21. Simulation result for output grid current with the proposed sensorless MPPT algorithm.

4.2. Configuration with Sensors

The classical method for MPPT using a perturb & observe algorithm with voltage and current measurements on the DC side shown in Figure 1b is simulated to determine the difference in performance between the proposed system and the classical single stage system with DC bus sensors. The simulation shown in Figure 22 shows that the response of the sensored configuration due to insolation changes and maximum power point tracking, is much faster than the proposed technique. This is due to the fact that the sensorless algorithms requires a low sampling rate in order to detect changes in m_a, whereas in the sensored configuration, the voltage and current change directly with the change in PV power and a high sampling rate may be used. Meanwhile, the sensorless algorithm current oscillations are minimized since when the system yields maximum power, the algorithm halts until changes occur. Whereas, the sensored technique in Figure 23 keeps on perturbing the system to determine changes in the maximum power which yields grid side current oscillations.

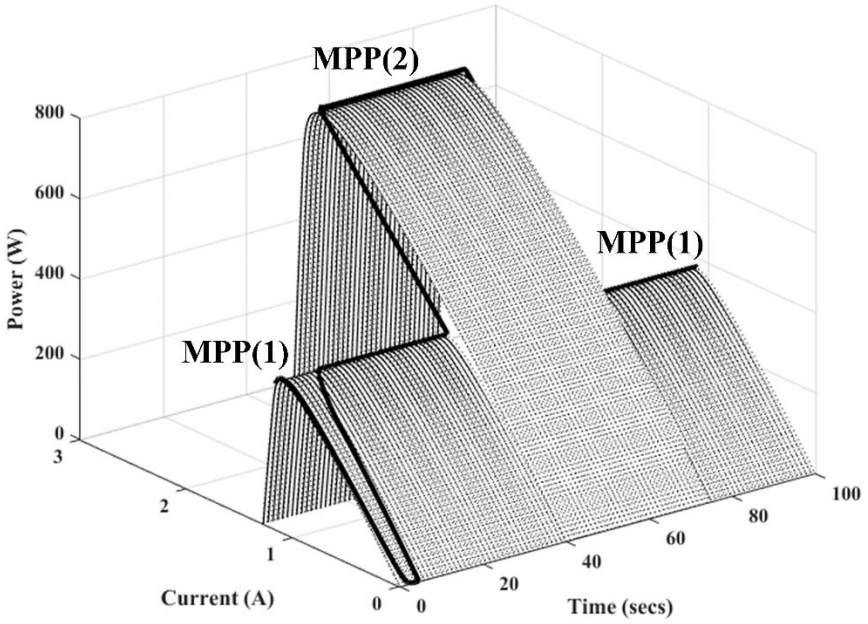

Figure 22. Simulation result of the classical sensored perturb and observe algorithm.

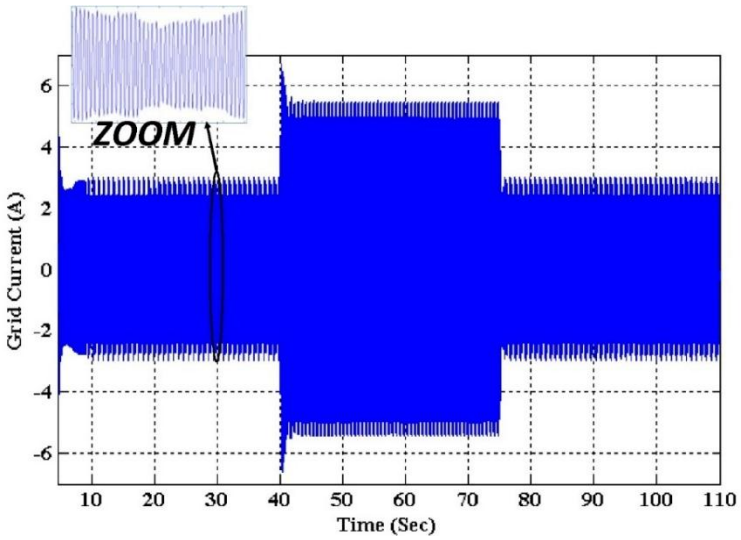

Figure 23. Simulation result for output grid current with the classical sensored perturb and observe algorithm.

4.3. Proposed Sensor-Less Configuration under Partial Shading

In order to further evaluate the performance of the proposed technique, the effect of partial shading is simulated. As shown in Figure 24a, partial shading is achieved by shading fifteen panels to an insolation of 500 W/m^2 while the remaining five are at maximum insolation of 1000 W/m^2. The result presented in Figure 24b shows that the algorithm is capable of tracking the maximum power without being affected by the presence of another power peak which shows he effectiveness of the algorithm under different operating conditions.

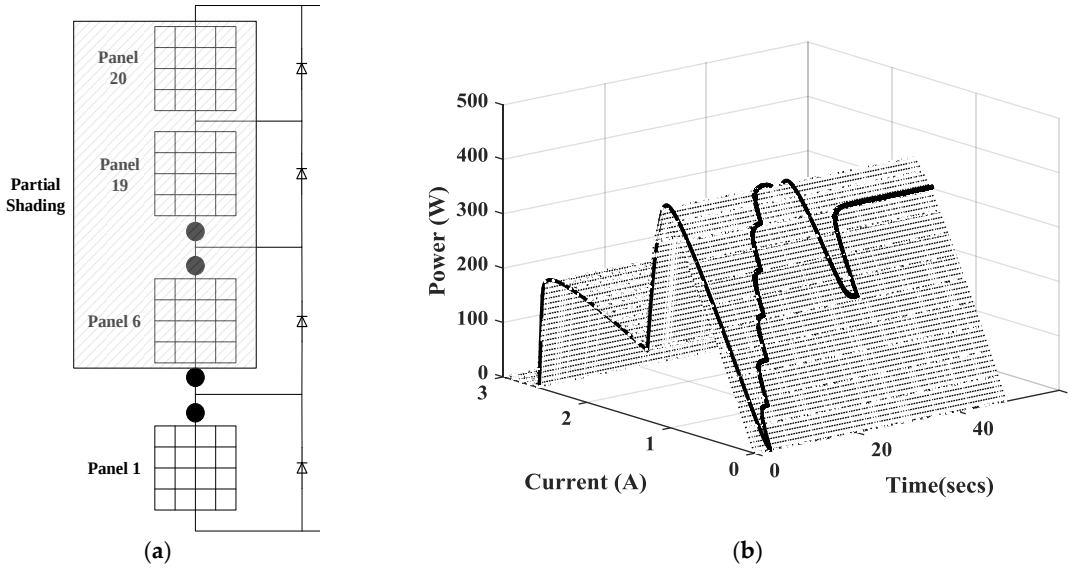

Figure 24. Partial shading of PV panels for 15 shaded panels at 5000 W/m^2 (**a**) connection configuration (**b**) simulation result.

4.4. Simulation Evaluation

In order to evaluate the difference between the proposed configuration and sensored configuration, Table 2 shows the performance of both techniques with respect to tracking time, output current oscillations and number of sensors used. As discussed previously, although the output current oscillations have been eliminated during steady state using the proposed algorithm, the tracking time is significantly larger. Trade-off between tracking time, output power quality and number of sensors utilized is of interest for further future research.

Table 2. Comparison between the proposed and classical configuration.

Tracking Time	Current Oscillations	Sensors	Configuration
26 s	0	2(V_g, I_g)	Proposed (Figure 9)
0.3 s	3.3%	4(V_{dc}, I_{dc}, V_g, I_g)	Classical (Figure 1b)

5. Experimental Results

The configuration was implemented on a system with the parameters in Table 3. A block diagram of the hardware setup is shown in Figure 25. A TMS320F28335 32-bit microcontroller (Texas Instruments, Dallas, TX, USA) was used as a controller and a Smart Power Module FSBB15CH60C (Fairchild Semiconductor International Inc., San Jose, CA, USA) as the inverter. A transformer was utilized to step up the output voltage of the inverter to match the grid voltage. The current transducer utilized is a CSNA111 50A Hall-effect current transducer (Honeywell, Morris Plains, NJ, USA) with a ratio of 50 A/50 mA while the voltage transducer utilized is a CYHVS025 voltage transducer (BBAUTOMACAO Inc., Long Island, NY, USA) with an input/output current of 10 mA/25 mA. The conditioning circuit converts the output current of each transducer from 0 to 3 V range which is suitable for the microcontroller analog to digital converter. The algorithm and current controller was developed and coded on the microcontroller using the Simulink Embedded Coder library under MATLAB.

Among the practical considerations, the controller considers m_a to be settled when m_a is within the *settlement range* for 10 consecutive algorithm samples. This is to ensure that oscillations during operation does not affect the judgement of considering m_a to be settled.

Table 3. Experimental system parameters.

Parameter	Value
V_g	220 V_{rms}
PV Panel Type	LORENTZ LC175-24M
Number of parallel PV Panels	2
P_{MPP}/panel	175 W at 1000 W/m^2
V_{MPP}	35 V at 1000 W/m^2
L_1	4 mH
C_{dc}	10 mF
Transformer ratio	7/230 V
Switching frequency & Current controller sampling frequency	10 kHz
Reference output power incremenet	15 W
Algorithm sampling rate	0.1 s

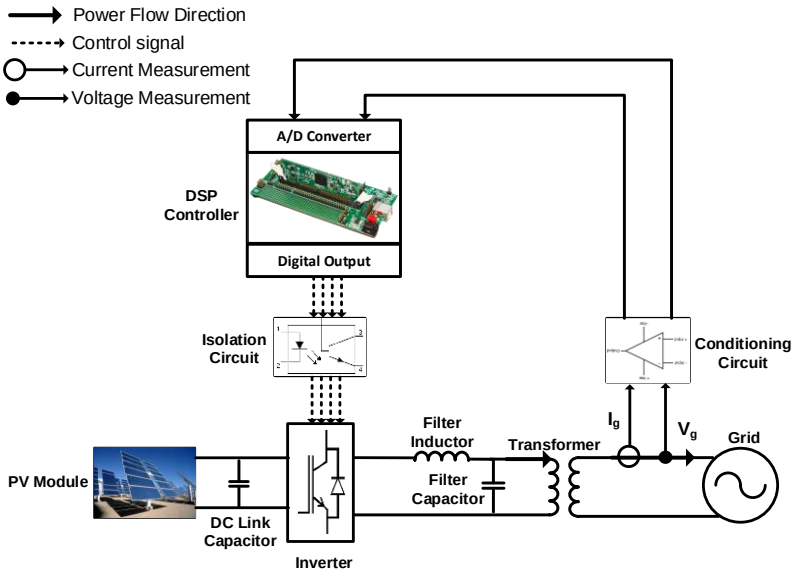

Figure 25. PV grid connected inverter hardware block diagram.

The output grid current waveform shown in Figure 26 was recorded on a digital oscilloscope and then redrawn. Figure 26 consists of eight operation regions, Region 1 is the off state before execution of the algorithm where the DC link capacitor is allowed to charge at the beginning of operation. In Region 2 the algorithm was executed and the Tracking Process is started. During each perturbation, the output grid current is increased as shown in Figure 27 while maintaining constant output until the algorithm ensures that m_a is settled for several algorithm execution cycles. The algorithm stops perturbing the output grid current at the end of Region 2 where m_a exceeds the maximum limit.

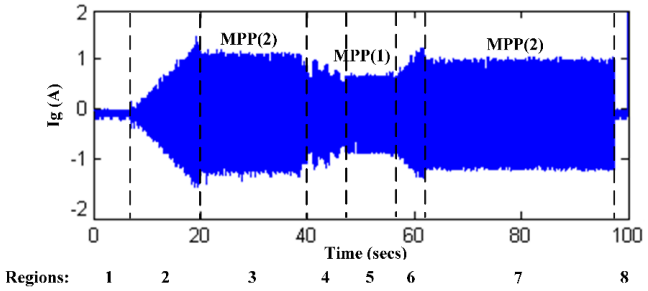

Figure 26. Experimental result of the output grid current using the sensorless algorithm.

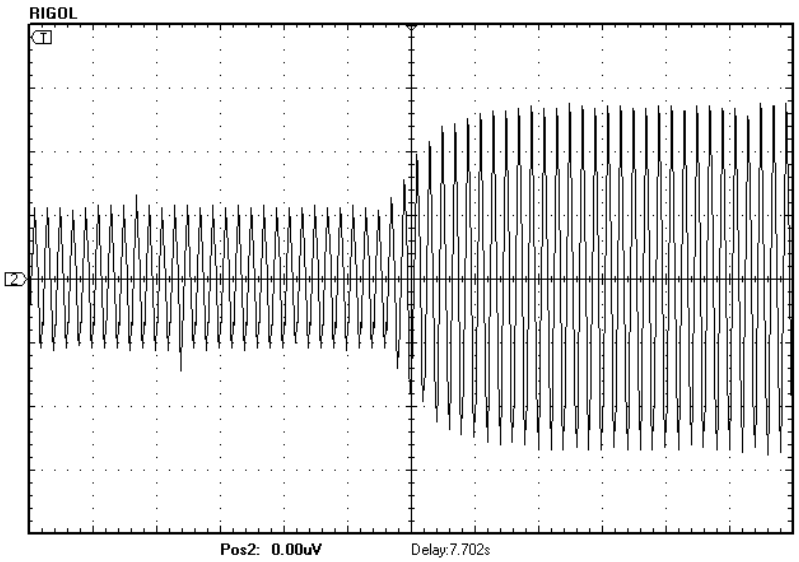

Figure 27. Increase in output grid current during perturbation in Region 2 (Vertical: 50 mA/div, Horizontal: 100 ms/div).

In Region 3, the algorithm shifts to Recharging Process and then to Observation Process where the algorithm moves directly to the previous output power noted by MPP(2) at which m_a was stable. Recharging Process is a quick process since P_{ref} is set to zero and the DC capacitor is immediately charged while m_a settles in less than the algorithm execution rate. It can be observed that the Tracking Process was concluded in approximately 12 s time span with a 15 W/step perturbation in P_{ref} and considering 1 s between each perturbation (0.1 s algorithm execution rate while waiting 10 consecutive cycles to ensure m_a settlement) the achieved P_{out} is 180 W and peak output current of 1.15 A as shown in Figure 26 in Region 3. However, the available P_{MPP} and absorbed power maybe greater due to inverter losses, filter losses and P_{ref} perturbation size. Moreover, it should be noted that the output current to the grid is always in phase with grid voltage as shown in Figure 28. In Figure 28, it can be observed that the current consists of minor switching harmonics. This is due to sizing of the inverter filter inductor which is a trade-off between filtering requirements and voltage drop across the inductor.

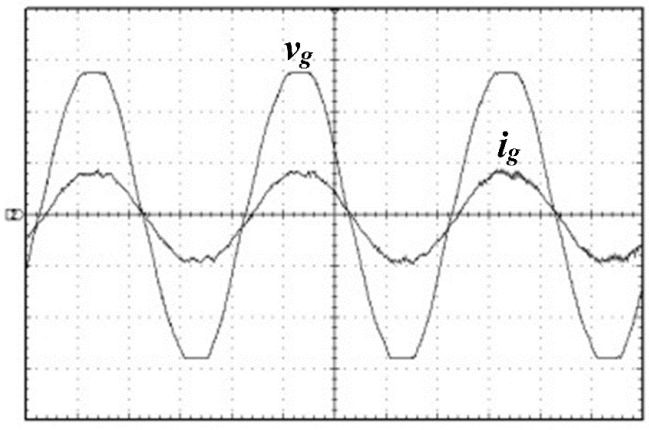

Figure 28. Grid current in phase with grid voltage during experimental operation in Region 2 (Vertical: v_g 100 V/div, i_g 1 A/div, Horizontal: 5 ms/div).

At 40 s, partial shading was applied to imitate the effect of decrease in solar insolation. The expected outcome is a reduction in available power and reduction in V_{dc} which leads to an

increase in m_a leading to instability and the algorithm shifts to Recharging Process as shown in Region 4. Region 4 shows execution of Recharging Process and when m_a was considered settled, the algorithm re-executed Tracking Process. The Tracking Process increments P_{ref} up to the new P_{MPP} then switches to Recharging Process followed by Observation Process while operating at MPP(1) in Region 5. The new P_{MPP} is achieved after 7 s of Tracking Process which indicates P_{out} is approximately 105 W and peak output current of 0.675 A as shown in Figure 26 in Region 5.

At 55 s, partial shading was removed to imitate the effect of an increase in solar insolation. Since the algorithm is in Observation Process, it immediately recognizes the decrease in m_a due to the increase in V_{dc} and Tracking Process is executed to determine the new P_{MPP} in Region 6. Similar to the sequence in Regions 2 and 3, once the new P_{MPP} is determined, the algorithm switches to Recharging Process then to Observation Process in Region 7 while operating at P_{MPP} of 180 W. Finally in Region 8 the controller was switched off.

It can be concluded from the experimental results that starting the *MPP* process with the proposed algorithm can be significantly slow. However, during operation and minor changes to operating conditions, the algorithm can track P_{MPP} significantly faster to the process start-up. Moreover, current oscillations during operation at P_{MPP} do not exist since the inverter operates at a constant P_{ref}. The results shows that the algorithm was able to track P_{MPP} during a transient disturbance for 15 s. Discontinuities can be considered minor since they occur during the Recharging Process which required 1 s during each disturbance. It should be noted that the process speed can be increased by having a fast current control loop such that the algorithm execution rate can be increased too since the main limitation in the algorithm speed is the determination of settlement of m_a.

6. Conclusions

A new sensor-less PV MPPT algorithm was developed and evaluated for a single-stage grid connected inverter. The algorithm showed good tracking capability under different operating conditions. The main contribution of the paper is the proposal of a sensor-less technique that can be simply implemented for any grid connected inverter without requirements of any hardware modifications to the setup for PV integration. Approaches utilizing the analyzed phenomena mainly concentrate on improving the performance of tracking which can add complexity to the control structure. Meanwhile, the proposed algorithm just requires the addition of a reference generation algorithm to the current controller and no addition of any extra external feedbacks. The main limiting disadvantage is the slow response of the system compared to a sensored algorithm. Interruptions in the output power occurs using the proposed algorithm merely after determining the maximum power. Later, during algorithm Observation Process the maximum power is set constant until changes to the operating conditions occur. Considering slow changes in operating conditions with regard to solar insolation and temperature, these interruptions are not comparable with continuous output power oscillations in classical techniques. However, as mentioned earlier, the technique lacks tracking speed which is not suitable for rapidly changing operating conditions and in such scenario the interruptions in energy production is an inevitable state. A trade-off between simplicity of the controller and tracking speed is a matter of further investigation. Future improvements to the algorithm can be achieved by utilizing artificial intelligence algorithms to learn such pattern changes and take appropriate action at a faster rate.

Acknowledgments: João Catalão and Edris Pouresmaeil thank the EU Seventh Framework Programme FP7/2007–2013 under grant agreement No. 309048, FEDER through COMPETE and FCT, under FCOMP-01-0124 -FEDER-020282 (Ref. PTDC/EEA-EEL/118519/2010), UID/CEC/50021/2013 and SFRH/BPD/102744/2014.

Author Contributions: All authors have worked on this manuscript together and all authors have read and approved the final manuscript.

Conflicts of Interest: The authors declare no conflict of interest.

References

1. Kjaer, S.B.; Pedersen, J.K.; Blaabjerg, F. A Review of single-phase grid-connected inverters for photovoltaic modules. *IEEE Trans Ind. Appl.* **2005**, *41*, 1292–1306. [CrossRef]
2. Marzband, M.; Parhizi, N.; Savaghebi, M.; Guerrero, J.M. Distributed smart decision-making for a multimicrogrid system based on a hierarchical interactive architecture. *IEEE Trans. Energy Convers.* **2015**, *99*, 1–12. [CrossRef]
3. Marzband, M.; Azarinejadian, F.; Savaghebi, M.; Guerrero, J.M. An optimal energy management system for islanded microgrids based on multiperiod artificial bee colony combined with Markov chain. *IEEE Syst. J.* **2015**, *99*, 1–11. [CrossRef]
4. Marzband, M.; Parhizi, N.; Adabi, J. Optimal energy management for stand-alone microgrids based on multi-period imperialist competition algorithm considering uncertainties: Experimental validation. *Int. Trans. Electr. Energy Syst.* **2015**. [CrossRef]
5. Marzband, M.; Yousefnejad, E.; Sumper, A.; Domínguez-García, J.L. Real time experimental implementation of optimum energy management system in standalone microgrid by using multi-layer ant colony optimization. *Int. J. Electr. Power Energy Syst.* **2015**, *75*, 265–274. [CrossRef]
6. Rahim, N.A.; Selvaraj, J.; Krismadinata. Hysteresis current control and sensorless MPPT for grid-connected photovoltaic systems. In Proceedings of the IEEE International Symposium on Industrial Electronics, Vigo, Spain, 4–7 June 2007; pp. 572–577.
7. Kitano, T.; Matsui, M.; Xu, D.H. Power sensor-less MPPT control scheme utilizing power balance at DC link-system design to ensure stability and response. In Proceedings of the 27th Annual Conference of the IEEE Industrial Electronics Society, Denver, CO, USA, 29 November–2 December 2001; pp. 1309–1314.
8. Park, S.S.; Jinda, A.K.; Gole, A.M.; Park, M.; Yu, I.K. An optimized sensorless MPPT Method for PV generation system. In Proceedings of the 2009 Canadian Conference on Electrical and Computer Engineering, St. John's, NL, USA, 3–6 May 2009; pp. 720–724.
9. Wu, L.B.; Zhao, Z.M.; Liu, J.Z.; Shu, L.; Yuan, L.Q. Modified MPPT strategy applied in single-stage grid-connected photovoltaic system. In Proceedings of the Eighth International Conference on Electrical Machines and Systems, Nanjing, China, 29 September 2005; pp. 1027–1030.
10. Ciobotaru, M.; Teodorescu, R.; Blaabjerg, F. Control of single-stage single-phase PV inverter. In Proceedings of the 2005 European Conference on Power Electronics and Applications, Dresden, Germany, 11–14 September 2005.
11. Phani Kiranmai, K.S.; Veerachary, M. A single-stage power conversion system for the PV MPPT application. In Proceedings of the IEEE International Conference on Industrial Technology, Mumbai, India, 15–17 December 2006; pp. 2125–2130.
12. Jain, S.; Agarwal, V. Comparison of the performance of maximum power point tracking schemes applied to single-stage grid-connected photovoltaic systems. *IET Electr. Power Appl.* **2007**, *1*, 753–762. [CrossRef]
13. Liu, F.; Zhou, Y.; Yin, J.; Duan, S. An improved MPPT arithmetic and grid-connected control strategy for single-stage three-phase PV converter with LCL filter. In Proceedings of the 3rd IEEE Conference on Industrial Electronics and Applications, Singapore, Singapore, 3–5 June 2008; pp. 808–813.
14. Li, D.; Gao, G.; Loh, P.C.; Wang, P.; Tang, Y. Transient maximum power point tracking for single-stage grid-tied inverter. *IEEE Energy Convers. Congr. Expo.* **2009**, 313–318. [CrossRef]
15. Wu, L.B.; Zhao, Z.M.; Liu, J.Z. A single-stage three-phase grid-connected photovoltaic system with modified MPPT method and reactive power compensation. *IEEE Trans. Energy Convers.* **2007**, *22*, 881–886.
16. Yu, W.L.; Lee, T.-P.; Wu, G.-H.; Chen, Q.S.; Chiu, H.-J.; Lo, Y.-K.; Shih, F. A DSP-based single-stage maximum power point tracking PV inverter. In Proceedings of the 2010 Twenty-Fifth Annual IEEE Applied Power Electronics Conference and Exposition (APEC), Palm Springs, CA, USA, 21–25 February 2010; pp. 948–952.
17. Lacerda, V.S.; Barbosa, P.G.; Braga, H.A.C. A single-phase single-stage, high power factor grid-connected PV system, with maximum power point tracking. In Proceedings of the 2010 IEEE International Conference on Industrial Technology (ICIT), Vina del Mar, Spain, 14–17 March 2010; pp. 871–877.
18. Patel, H.; Agarwal, V. MPPT scheme for a PV-fed single-phase single-stage grid-connected inverter operating in CCM with only one current sensor. *IEEE Trans. Energy Convers.* **2009**, *24*, 256–263. [CrossRef]

19. Elsaharty, M.A.; Hamad, M.S.; Ashour, H.A. Digital hysteresis current control for grid-connected converters with LCL filter. In Proceedings of the 37th Annual Conference on IEEE Industrial Electronics Society, Melbourne, Australia, 7–10 November 2011; pp. 4685–4690.
20. Hu, H.B.; Harb, S.; Kutkut, N.H.; Shen, Z.J.; Batarseh, I. A single-stage microinverter without using eletrolytic capacitors. *IEEE Trans. Power Electron.* **2013**, *28*, 2677–2687. [CrossRef]
21. Villalva, M.G.; Gazoli, J.R.; Filho, E.R. Comprehensive approach to modeling and simulation of photovoltaic arrays. *IEEE Trans. Power Electron.* **2009**, *24*, 1198–1208. [CrossRef]
22. Pouresmaeil, E.; Montesinos-Miracle, D.; Gomis-Bellmunt, D. Control scheme of three-level h-bridge converter for interfacing between renewable energy resources and AC grid. In Proceedings of the 14th European Conference on Power Electronics and Applications, Birmingham, UK, 30 August–1 September 2011; pp. 1–9.
23. Elsaharty, M.A.; Ashour, H.A. Realization of DC-bus sensor-less MPPT technique for a single-stage PV grid-connected inverter. In Proceedings of the 23rd International Conference and Exhibition on Electricity Distribution, Lyon, France, 15–18 June 2015; p. 204.
24. Nousiainen, L.; Puukko, J.; Mäki, A.; Messo, T.; Huusari, J.; Jokipii, J.; Viinamäki, J.; Lobera, D.T.; Valkealahti, S.; Suntio, T. Photovoltaic generator as an input source for power electronic converters. *IEEE Trans. Power Electron.* **2013**, *28*, 3028–3038. [CrossRef]
25. Urtasun, A.; Sanchis, P.; Marroyo, L. Adaptive voltage control of the DC/DC boost stage in PV converters with small input capacitor. *IEEE Trans. Power Electron.* **2013**, *28*, 5038–5048. [CrossRef]
26. Khanna, R.; Zhang, Q.H.; Stanchina, W.E.; Reed, G.F.; Mao, Z.H. Maximum power point tracking using model reference adaptive control. *IEEE Trans. Power Electron.* **2014**, *29*, 1490–1499. [CrossRef]
27. Liu, L.; Li, H.; Xue, Y.; Liu, W. reactive power compensation and optimization strategy for grid-interactive cascaded photovoltaic systems. *IEEE Trans. Power Electron.* **2015**, *30*, 188–202.
28. Pouresmaeil, E; Jorgensen, B.N.; Veje, C.; Catalao, J.P.S. A flexible control strategy for integration of DG sources into the power grid. In IEEE Proceedings of the Australasian Universities Power Engineering Conference (AUPEC), Perth, Australia, 28 September–1 October 2014; pp. 1–6.
29. Mehrasa, M.; Adabi, E.; Pouresmaeil, E.; Adabi, J. Passivity-based control technique for integration of DG resources into power grid. *Int. J. Electr. Power Energy Syst.* **2014**, *58*, 281–290. [CrossRef]
30. Mehrasa, M.; Pouresmaeil, E.; Mehrjerdi, H.; Jørgensen, B.N.; Catalao, J.P.S. Control technique for enhancing the stable operation of distributed generation units within a microgrid. *Energy Convers. Manag.* **2015**, *97*, 362–373. [CrossRef]
31. Pouresmaeil, E.; Akorede, M.F.; Hojabri, M. A hybrid algorithm for fast detection and classification of voltage disturbances in electric power systems. *Eur. Trans. Electr. Power* **2011**, *21*, 555–564. [CrossRef]
32. Elsaharty, M.A.; Ashour, H.A. Passive L and LCL filter design method for grid-connected inverters. In Proceedings of the IEEE Innovative Smart Grid Technologies, Kuala Lumpur, Malaysia, 20–23 May 2014.